A First-Principles-Based Microkinetic Study of CO<inf>2</inf>Reduction to CH<inf>3</inf>OH over In<inf>2</inf>O<inf>3</inf>(110)

ACS Catalysis

pubs.acs.org/acscatalysis

Research Article

A First-Principles-Based Microkinetic Study of CO_2 Reduction to CH_3OH over $In_2O_3(110)$

Alvaro Posada-Borbón* and Henrik Grönbeck*

Cite This: *ACS Catal.* 2021, 11, 9996−10006

Read Online

ACCESS | Metrics & More | Article Recommendations | Supporting Information

ABSTRACT: Methanol synthesis from catalytic recycling of CO_2 is one viable route to produce fuel and a stock chemical from a greenhouse gas. Herein, hydrogenation of CO_2 to CH_3OH is investigated with density functional theory calculations combined with mean-field microkinetic modeling. The model explores the direct route for CO_2 hydrogenation (HCOOH route) and the competing reverse water-gas shift (RWGS) reaction. The predicted temperature dependence of turnover frequencies, selectivities, and reaction orders are in good agreement with previous experimental results. The formation of methanol at relevant reaction temperatures (470−670 K) is found to be kinetically controlled by H_2COOH dissociation to H_2CO + OH, whereas the RWGS reaction is solely controlled by CO_2 hydrogenation to COOH. An analysis of the kinetic behavior reveals that the stabilization of hydrogen adsorption should be one way to improve the catalyst performance.

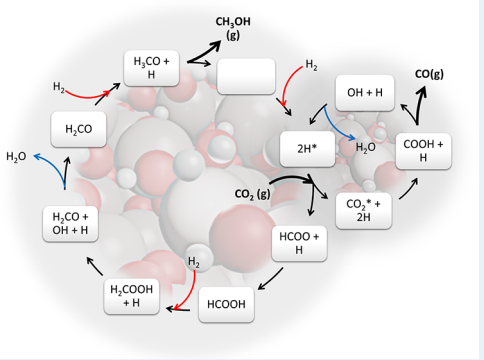

KEYWORDS: *first-principles microkinetic modeling, methanol synthesis, selectivity, CO_2 hydrogenation, In_2O_3*

INTRODUCTION

Alternative energy sources to fossil fuels are generally limited by their fleeting capacity of storing energy. An attractive solution is to store energy in chemical bonds of molecules that are easy to handle on the industrial scale, such as methanol (CH_3OH). The synthesis of methanol by catalytic recycling of CO_2, coupled with a sustainable production of H_2, is one viable route for sustainable production of a fuel with high energy density and a valuable stock chemical.[1−5] The need for efficient CO_2 hydrogenation catalysts has sparked considerable efforts to find systems with high activity and selectivity.[6−19]

The catalytic synthesis of CH_3OH is currently performed industrially via a $CO/CO_2/H_2$ mixture over $Cu/ZnO/Al_2O_3$, at temperatures and pressures of 470−570 K and 50−100 bar.[8,13,20] The process requires a large-scale operation, and the catalyst has limited selectivity and deactivates over time due to copper sintering.[21,22] In_2O_3-based catalysts for CO_2 reduction to methanol have recently attracted significant attention, thanks to their high activity, selectivity, and durability.[12,23−28] Early computational[29] and experimental[12] works have suggested that oxygen vacancies (O_v) facilitate the reaction by promoting activation of the reactants. In ref 12, the relative percentage of oxygen vacancies (O_v) was estimated from X-ray photoelectron spectroscopy (XPS) measurements and a relation between the presence of vacancies and activity was suggested.[12] It should, however, be noted that the estimation of vacancy concentration from measurements of O 1s core level binding energies is not straightforward, as the suggested XPS signature of O_v is in the energy region of different types of OH groups.[30]

Particularly good performance for In_2O_3-based catalysts has been reported for In_2O_3 supported on ZrO_2[12,25,26,31] and Pd-doped In_2O_3.[24] A proposed underlying reason for the improved activity of In_2O_3/ZrO_2 is a higher amount of oxygen vacancies.[12] However, the amount of O_v in ZrO_2-supported In_2O_3 is reported to be lower (14−15%) than for the unsupported In_2O_3 (16−24%), which indicates that the concentration of vacancies is not the only parameter that controls the activity. Another suggestion for the improved activity of In_2O_3/ZrO_2 is the creation of $In{:}ZrO_2$ sites ($In{-}O_v{-}Zr$),[27] which contains a vacancy and simultaneously hinders over-reduction of the In_2O_3 phase. Over-reduction is known to result in fast degradation.[27] The enhanced performance upon Pd doping has been suggested to originate from facile H_2 dissociation.[23]

Computational first-principles insight of CO_2 hydrogenation to methanol over In_2O_3 has been obtained on a range of surfaces, including bixbyite $In_2O_3(110)$,[29,32] $In_2O_3(111)$,[23,32] and hexagonal $In_2O_3(104)$[33,34] and $In_2O_3(012)$.[34] In ref 29, CO_2 hydrogenation to methanol was investigated by density functional theory (DFT) calculations on $In_2O_3(110)$. The reaction was proposed to follow a Mars−van Krevelen mechanism, where H_2 creates an oxygen vacancy, which

Received: April 14, 2021
Revised: July 13, 2021
Published: July 27, 2021

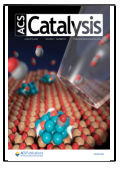

becomes the active site for the reactions. The hydrogenation is proposed to proceed according to $CO_2 \rightarrow HCOO^* \rightarrow H_2COO^* \rightarrow H_3CO^* \rightarrow CH_3OH^*$. As the highest energy barrier in the catalytic cycle is hydrogenation of H_2CO to H_3CO, this step has been suggested to be rate limiting.[29] Very recently,[32] the same mechanism was interrogated by DFT-based mean-field microkinetic modeling over both $In_2O_3(110)$ and $In_2O_3(111)$. These simulations suggest that the rate-determining step is the hydrogenation of formate $HCOO \rightarrow H_2COO$ on $In_2O_3(110)$ and dissociation of hydrogen on $In_2O_3(111)$.[32] The simulations, however, fail to describe the experimental observation that the rate of CO production is higher than that of methanol production at high temperatures.[32] The importance of a Mars–van Krevelen step was explored also in ref 33 for the reaction over hexagonal $In_2O_3(104)$. It was found that oxygen vacancies on hexagonal $In_2O_3(104)$ stabilize reaction intermediates to a larger extent than on the bixbyite surfaces, which was correlated with the observed improvement of the overall activity and selectivity with respect to the bixbyite phase.[33] A variation of the mechanism in ref 29, including the adsorption of CO_2 on an In ion, was investigated for hexagonal $In_2O_3(104)$ and $In_2O_3(012)$,[34] showing kinetic behavior similar to that in ref 32.

$In_2O_3(111)$ is known to be the stable surface of bixbyite In_2O_3, and a DFT-based microkinetic model of CO_2 reduction to CH_3OH over $In_2O_3(111)$ was presented in ref 23. The reaction was proposed to occur near an O_v site, and the hydrogenation was suggested to follow the route $CO_2 \rightarrow HCOO^* \rightarrow HCOOH^* \rightarrow H_2COOH^* \rightarrow H_2COHOH^* \rightarrow H_2CO^* \rightarrow H_3CO^* \rightarrow CH_3OH^*$. The simulations show good agreement with experiments with respect to reaction orders but do not describe the experimentally observed preference for CO production at higher temperatures with respect to methanol production.

The previous first-principles studies of CO_2 hydrogenation over In_2O_3 surfaces consider the reaction in the limit of low hydrogen coverage.[23,29,32−34] However, it is known that In_2O_3 surfaces are easily hydroxylated[35] and DFT-based analyses of the thermodynamic stability of $In_2O_3(110)$ and $In_2O_3(111)$ suggest that the surfaces are heavily hydroxylated under typical methanol synthesis conditions.[36,37] The hydroxylation was reported to induce a change in oxidation state (In^{3+} to In^+) of undercoordinated In ions, making them important for the reaction by facilitating CO_2 activation.[36]

Herein, a mean-field microkinetic model is constructed based on DFT calculations to analyze CO_2 hydrogenation to methanol. The reaction is considered over a hydroxylated $In_2O_3(110)$ surface in the absence of oxygen vacancies. The simulated kinetic behavior is found to describe the experimental temperature dependence of turnover frequencies, selectivities and reaction orders of CO_2, H_2, and H_2O. The rate-determining step is found to be $H_2COOH^* \rightarrow H_2CO^* + OH^*$ at all relevant temperatures. Additionally, it is found that stabilizing the adsorption of hydrogen significantly increases the methanol production.

COMPUTATIONAL METHODS

DFT Calculations. Density functional theory (DFT) calculations were performed using the Vienna *ab initio* simulation package (VASP).[38−41] The exchange correlation energy was obtained using the Perdew, Burke, Ernzerhof (PBE) formulation.[42] A plane-wave basis was used to expand the Kohn–Sham orbitals, truncated at a kinetic energy of 500 eV. The interaction between the valence electrons and the core was described with projector augmented wave potentials (PAW).[43,44] Hydrogen, carbon, oxygen, and indium were described with 1, 4, 6, and 13 valence electrons, respectively. Brillouin zone integration is approximated by finite sampling, using the Monkhorst–Pack scheme.[45] A k-point grid of $3 \times 3 \times 1$ was used for the surface calculations. The total energy was considered to be converged when the difference between steps in the electronic optimization was smaller than 10^{-6} eV. Structural optimization was performed by use of the conjugate gradient method, and convergence was assumed when the forces were smaller than 0.01 eV/Å. Activation energies were calculated using the climbing-image nudge elastic band (CI-NEB) technique.[46] Six to ten images were used along the reaction coordinate to describe the minimum-energy path. A force criterion of 0.05 eV/Å was used in the search for the transition states,[37] and the saddle points were confirmed by a vibrational analysis. Vibrational energies were calculated within the harmonic approximation, using finite differences with displacements of 0.015 Å.

$In_2O_3(110)$ was modeled with a (1×1) surface cell and described with four atomic layers. The bottom two layers were fixed to their bulk positions during the geometry optimizations. The slabs were separated by at least 15 Å of vacuum. The convergence criteria in kinetic energy, k points, and vacuum were found to sufficiently describe the adsorption energy of the HCOOH intermediate within at least 0.02 eV. Gas-phase molecules were optimized in a $11 \times 12 \times 13$ Å simulation box.

Gas-phase energies of O–C–O- and OH-containing species are known to be poorly described using semilocal functionals such as PBE,[11,47,48] yielding in some cases substantial errors in the overall reaction energy. Here, the total energies of CO_2, CO, H_2, H_2O, and CH_3OH were corrected to properly describe the enthalpy changes of the reactions ($CO_2 + 3H_2 \rightarrow CH_3OH + H_2O$, $\Delta H_f^{298K} = -0.55$ eV; $CO + H_2O \rightarrow CO_2 + H_2$, $\Delta H_f^{298K} = 0.43$ eV). We followed the procedure outlined in refs 11 and 47, and the details are reported in the Supporting Information. The gas-phase correction aligns the equilibrium constants for the methanol synthesis and RWGS reactions to the experimental values. With the corrections, the enthalpy changes were calculated to be $\Delta H_f = -0.56$ eV and $\Delta H_f = 0.42$ eV for the methanol and RWGS reactions, respectively. The gas-phase corrections affected the surface coverages and temperature for the maximum of the TOF. The results for microkinetic simulations without corrections are presented in Figures S5 and S6 in the Supporting Information.

Microkinetic Modeling. The reaction kinetics were treated within the mean-field approximation. Hence, the rate of the elementary reactions was assumed to be proportional to the surface coverage of the species involved in the reaction. This approach gave rise to a set of coupled ordinary differential equations for the surface coverages. The coverage evolution in time of each surface specie was calculated according to

$$\frac{d\theta_i}{dt} = \sum_j c_{ij} r_j(\vec{\theta}) \tag{1}$$

where θ_i is the coverage of the ith species, c_{ij} is the number of i molecules consumed in reaction j, and $r_j(\vec{\theta})$ is the surface-coverage-dependent reaction rate for the jth reaction. The system of equations was solved by numerical integration using the Scipy ODE solver for the initial value problem with the backward differentiation formula (BDF) method.[49] The

https://doi.org/10.1021/acscatal.1c01707
ACS Catal. 2021, 11, 9996−10006

integration was performed until a steady state was reached for all reactions.

The rate constant k for the adsorption reactions was calculated from kinetic gas theory as[50]

$$k_i^{\mathrm{ads}} = \frac{p_i A_{\mathrm{site}}}{\sqrt{2\pi m_i k_B T}} \exp\left(-\frac{\Delta E_a}{k_B T}\right) \tag{2}$$

The subscript i denotes the adsorbing species, and p_i is the corresponding gas-phase pressure. A_{site} is the surface area of an adsorption site (set to 10 Å^2), m_i is the molecular mass of the adsorbing species, k_B is Boltzmann's constant, T is the temperature, and ΔE_a is the activation energy. Thermodynamic consistency between adsorption and desorption was guaranteed by calculating the desorption rate constant (k_i^{des}) from the forward rate constant (k_i^{ads}) and the equilibrium constant (K_i) according to

$$k_i^{\mathrm{des}} = \frac{k_i^{\mathrm{ads}}}{K_i} = k_i^{\mathrm{ads}} \exp\left(\frac{\Delta G_i(T,p)}{k_B T}\right) \tag{3}$$

where ΔG_i is the change in Gibbs free energy upon adsorption. Entropy contributions to Gibbs free energy in the gas phase were obtained from thermodynamic tables,[51] whereas the entropy of adsorbed species was calculated within the harmonic approximation.

Rate constants for the surface reactions were calculated with harmonic transition state theory as[52]

$$k_{\mathrm{TST}} = \frac{k_B T}{h} \frac{q_0^{\ddagger}}{q} \exp\left(-\frac{\Delta E_a}{k_B T}\right) \tag{4}$$

where h is Planck's constant, $q_0^{\ddagger}$ is the partition function (without the reaction coordinate) of the transition state aligned to the zero energy of the initial state, q is the partition function of the initial state, and ΔE_a is the activation energy. $q_0^{\ddagger}$ and q were evaluated in the harmonic approximation.

The reaction orders (n_i) and degrees of rate control (χ_i) were calculated to investigate the kinetic behavior of the explored mechanism. The reaction order is calculated as[50]

$$n_i = p_i \frac{\partial \ln r_x}{\partial p} \tag{5}$$

where p_i is the pressure of the molecular species of interest and r_x is the net rate of the reaction. For methanol synthesis, we investigated the reaction orders of CO_2, H_2, H_2O, and CH_3OH. The degree of rate control (χ_i) provides a way to investigate the sensitivity of total rate on the elementary steps in the reaction mechanism. The degree of rate control is defined as[53]

$$\chi_i = \frac{k_i}{r_x}\left(\frac{\partial r_x}{\partial k_i}\right)_{K_i} \tag{6}$$

where k_i is the rate constant of the elementary reaction step i, r_x is the net reaction rate, and K_i is the equilibrium constant of the ith elementary step. The derivative was taken with respect to the rate constant, with K_i kept unchanged. Operationally, this was done by a numerical differentiation of the rate with respect to the rate constant, performed by changing the rate constant by 1%. A positive value of χ_i indicates a rate-controlling step, whereas a negative value indicates inhibition. The step is rate determining in case χ_i is equal to 1.[53] Additionally, a sum rule exists, where the sum over all χ_i values equals unity.

RESULTS

Model Surface. First-principles thermodynamic calculations suggest that $In_2O_3(110)$ is hydroxylated under typical methanol synthesis conditions.[36,37] This is in accord with experimental observations of low-temperature (<400 K) reduction of In_2O_3 powder samples in dry H_2 and facile replenishment of oxygen vacancies by traces of water.[54] Moreover, water has been measured to dissociate on $In_2O_3(111)$ at room temperature, forming ordered hydroxyl overlayers.[35]

Here we consider the reaction over $In_2O_3(110)$ (see Figure 1). The surface cell consists of stoichiometric layers, where each

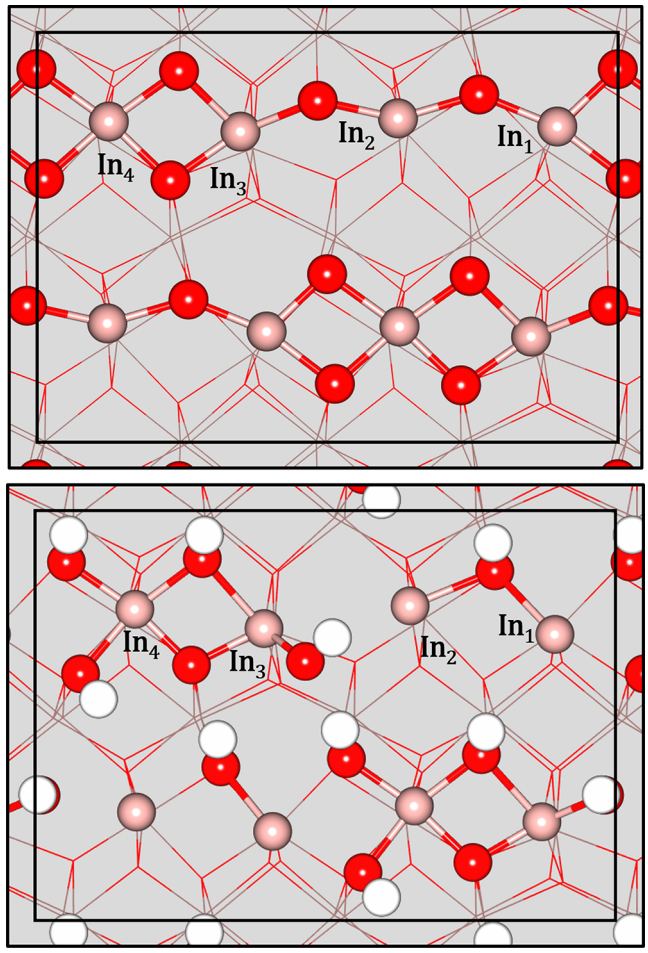

Figure 1. Structural model of pristine (top) and 83% H covered (bottom) $In_2O_3(110)$. A ball and stick model is used to show the adsorbates and topmost In and O atoms, whereas the rest are represented by lines. Atomic color code: indium (brown), oxygen (red), hydrogen (white).

layer contains two chains with six and four nonequivalent oxygen and indium ions, respectively. The oxygen ions are 3-fold coordinated. Half of the indium ions are 4-fold coordinated (In_1, In_2), whereas those of the other half are 5-fold coordinated (In_3, In_4). We consider the hydroxylated surface with a hydrogen coverage of 83%, which is calculated to be the equilibrium coverage under typical reaction conditions.[36] The coverage corresponds to five dissociated H_2 molecules in the surface cell (Figure 1), forming OH groups. The formation of OH groups changes the oxidation states from In^{3+} to In^{+} for the 4-fold coordinated In ions and one of the 5-fold coordinated In ions

https://doi.org/10.1021/acscatal.1c01707
ACS Catal. 2021, 11, 9996−10006

(In_3).[36] The change in oxidation state facilitates CO_2 adsorption and activation.[36] Further hydroxylation from this coverage occurs by heterolytic dissociation and formation of an InH−OH pair.

It is clear that the exact degree of hydroxylation fluctuates during the reaction. In fact, the considered state in Figure 1 is energetically close to a structure containing one oxygen vacancy.[37] Here, we chose to investigate the reaction with the equilibrium coverage as the starting point, which is convenient, as the number of possible configurations is limited once the H_2 molecules that take part in the reaction are adsorbed. Given the importance of hydroxylation on the oxidation states of In, we believe that the reaction should be studied at high hydrogen coverage.

Catalytic Cycle. The considered reaction mechanism includes a direct pathway for CO_2 hydrogenation to CH_3OH and a pathway for the reverse water-gas shift reaction. The hydrogenation of CO_2 to methanol is considered to proceed according to $CO_2 \rightarrow HCOO^* \rightarrow HCOOH^* \rightarrow H_2COOH^* \rightarrow H_2CO^* \rightarrow H_3CO^* \rightarrow CH_3OH^* \rightarrow CH_3OH$. This reaction pathway is regarded as a viable route on Cu-based catalysts.[7,11,16,47] The RWGS reaction is considered to occur according to $CO_2 \rightarrow CO_2^* \rightarrow COOH^* \rightarrow CO$. A schematic of the catalytic cycle is shown in Figure 2.

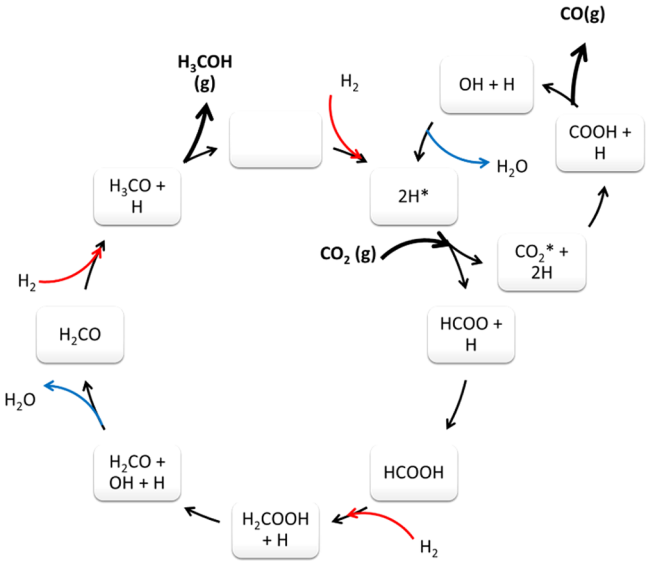

Figure 2. Schematic of the investigated catalytic cycle for CO_2 hydrogenation and the RWGS over $In_2O_3(110)$. Hydrogen adsorption (water desorption) steps are indicated by red (blue) arrows. The empty box at the top of the main cycle represents the surface without reactants or products.

The two reactions proceed along paths where the intermediate surface species are formally either neutral (HCOOH, H_2CO) or anions (HCOO, COOH, H_2COOH, H_3CO). The formation of charged surface species has consequences for reaction paths on oxide surfaces, given the importance of electronic pairing.[55] The reaction for In_2O_3 should presumably proceed to retain the oxidation state of the In ions to be either In^{3+} or In^+. (The In^{2+} state is unfavorable according to the inert-pair effect.)

The proposed mechanism is constructed with respect to the relative stability of the intermediates, where the most stable intermediates are considered to take part in the reaction. The energy of the most stable configuration for the tested intermediates is presented in Table S3 in the Supporting Information.

Energy Landscape. The zero point energy corrected potential energy diagrams for both reactions are presented in Figure 3a together with the Gibbs free energy in Figure 3b. The entropic contributions are calculated at 573 K with p_x = 30:10:1:1:1 bar for x = H_2:CO_2:H_2O:CH_3OH:CO. The structures of selected intermediates are presented in Figure 3c. All reaction intermediates and transition-state structures are reported in the Supporting Information.

The initial configuration for both reactions is the hydroxylated $In_2O_3(110)$ with an H coverage of 83% and $3H_2$ and CO_2 in the gas phase. H_2 adsorbs dissociatively in a heterolytic, fashion forming an InH−OH pair. The barrier is 0.84 eV, and the reaction is slightly exothermic (−0.02 eV). H_2 at this coverage is dissociated heterolytically ($H^- + H^+$), as the remaining In^{3+} ions are not uncoordinated enough to allow for an In^{3+} to In^+ reduction. The reaction proceeds from the InH−OH state by hydrogen diffusion to an OH−OH state, which is endothermic by 0.19 eV. The reaction splits at this step into (i) CO_2 hydrogenation to CH_3OH and (ii) the RWGS shift reaction.

CO_2 Hydrogenation to CH_3OH. From the OH + OH configuration, there is a second hydrogen diffusion step leading to a second InH−OH configuration. This step is endothermic by 0.26 eV. CO_2 is introduced in this configuration as a physisorbed species. The physisorption is exothermic by −0.09 eV. CO_2 hydrogenation to formate (HCOO) occurs with an energy barrier of 0.17 eV, by picking up a hydrogen from the In−H hydride. Formate is adsorbed in a bridge configuration between In sites (Figure 3c). CO_2 is hydrogenated from the InH site as it supports the (formal) transfer of H^- to form $HCOO^-$. The first hydrogenation step is exothermic by −1.17 eV. The reaction proceeds with a rotation of formate to a position where an O atom is located over an OH group in the $In_2O_3(110)$ trench. This rotation is endothermic by 0.17 eV. The second hydrogenation step occurs by a transfer of a proton from the OH group, forming HCOOH (Figure 3c). The process has an energy barrier of 0.72 eV and is endothermic by 0.65 eV.

The surface H coverage is 83% after the two hydrogenation steps, and we allow for adsorption of the second H_2 following the same dissociative path as for the first H_2 molecule. The heterolytic adsorption of hydrogen does not affect the stability of HCOOH. An endothermic (0.20 eV) rotation of HCOOH takes place to allow for the third hydrogenation step. Here, HCOOH picks up H^- from the In−H site, forming H_2COOH^- (Figure 3c). The activation energy for this step is 0.24 eV, and the reaction is exothermic by −0.32 eV. H_2COOH^- is adsorbed in a bridging configuration between two In sites. The following step is the dissociation of H_2COOH^- to $H_2CO + OH^-$ (Figure 3c). The dissociation takes place over an In ion, forming a surface OH group. This step has the highest barrier in the hydrogenation process, being 0.90 eV, and the dissociation is endothermic by 0.25 eV. The following step is the formation of water from an In-bound OH group and a surface OH group. This process is virtually barrierless and slightly exothermic. The desorption of water is endothermic by 0.69 eV and leaves H_2CO bridging two In ions on the surface. The reverse reaction of water adsorption is barrierless. The third heterolytic H_2 adsorption is found to stabilize the adsorbed H_2CO by 0.44 eV by the formation of additional hydrogen bonds. The formation of an OH−OH configuration is endothermic by 0.05 eV and induces a rotation of H_2CO to a configuration

https://doi.org/10.1021/acscatal.1c01707
ACS Catal. 2021, 11, 9996−10006

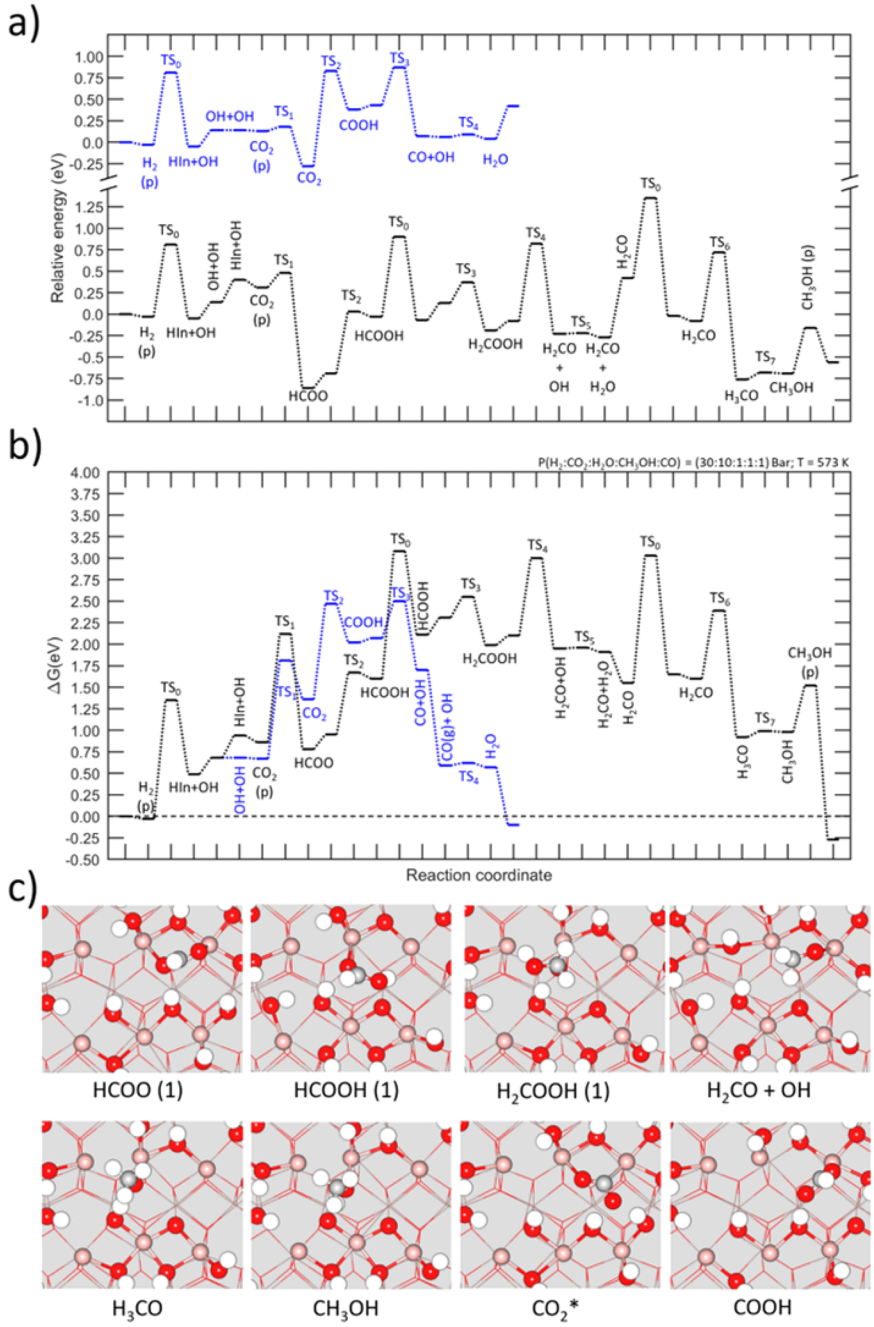

Figure 3. (a) Zero point energy corrected potential energy diagram. (b) Gibbs free energy diagram at 573 K and p_x = 30:10:1:1:1 bar for x = H_2:CO_2:H_2O:CH_3OH:CO. (c) Ball-and-stick models of relevant reaction intermediates (carbon is shown in gray). The atomic color code is the same as that in Figure 1.

across the trench bridging two In atoms. The hydrogenation of H_2CO to H_3CO occurs by the transfer of one hydrogen atom from a surface OH group. This step has a barrier of 0.79 eV and is exothermic by −0.68 eV. H_3CO is adsorbed in a monodentate configuration (Figure 3c). The final hydrogenation step from H_3CO to CH_3OH (Figure 3c) proceeds by transfer of a hydrogen atom from a surface OH group. This step has a barrier of 0.08 eV and is endothermic by 0.07 eV. The desorption of CH_3OH to a physisorbed state is endothermic by 0.53 eV. By rearrangement of the OH groups on the surface, the final state with CH_3OH and H_2O in the gas phase is exothermic by −0.40 eV. The reverse reaction of methanol adsorption is barrierless. The hydrogenation of formate (HCOO) to dioxymethylene (H_2COO) was also investigated. However, despite the comparable stabilities of dioxymethylene and formate, an energy barrier of 1.4 eV is calculated for its formation, which is too high to be competitive with the formation of formic acid from HCOO, having a barrier of 0.7 eV. Hence, the H_2COO pathway was not explored further.

Reverse Water-Gas Shift Reaction. At the initial OH + OH configuration in the potential energy diagram, CO_2 is introduced to the system as a physisorbed molecule. From the physisorbed state, CO_2 adsorbs onto on In ion in a CO_2^- configuration (Figure 3c). This process has an energy barrier of 0.05 eV and is exothermic by −0.41 eV.

https://doi.org/10.1021/acscatal.1c01707
ACS Catal. 2021, 11, 9996−10006

Table 1. Reaction Network and Calculated Kinetic Parameters: Elementary Steps and Zero Point Energy Corrected Forward (E_f) and Backward (E_b) Activation Energies and Pre-exponential Factors[a]

no.	reaction	E_f (eV)	E_b (eV)	A_f	A_b
R_1	$H_2(g) + 2^* \leftrightarrow 2\ H^*$	0.84	0.86	8.3×10^3	9.5×10^9
R_2	$CO_2(g) + H^* \leftrightarrow HCOO^*$	0.17	1.34	1.8×10^3	4.2×10^{13}
R_3	$HCOO^* + H^* \leftrightarrow HCOOH^* + *$	0.72	0.07	5.9×10^{12}	1.9×10^{12}
R_4	$HCOOH^* + H^* \leftrightarrow H_2COOH^* + *$	0.24	0.55	3.9×10^{11}	1.9×10^{13}
R_5	$H_2COOH^* + * \leftrightarrow H_2CO^* + OH^*$	0.90	1.05	5.3×10^{13}	2.7×10^{13}
R_6	$OH^* + H^* \leftrightarrow H_2O + *$	0.02	0.05	4.2×10^{12}	3.9×10^{12}
R_7	$H_2CO^* + H^* \leftrightarrow H_3CO^* + *$	0.79	1.47	7.6×10^{12}	2.7×10^{12}
R_8	$H_3CO^* + H^* \leftrightarrow CH_3OH^* + *$	0.08	0.01	7.1×10^{12}	2.0×10^{13}
R_9	$CO_2(g) + * \leftrightarrow CO_2^*$	0.05	0.46	1.8×10^3	4.2×10^{13}
R_{10}	$CO_2^* + H^* \leftrightarrow COOH^* + *$	1.11	0.45	2.4×10^{13}	8.2×10^{11}
R_{11}	$COOH^* \leftrightarrow CO(g) + OH^*$	0.44	0.80	7.1×10^{12}	2.2×10^3
R_{12}	$H_2O^* \leftrightarrow H_2O(g) + *$	0.69	0.10	2.9×10^{12}	2.8×10^3
R_{13}	$CH_3OH^* \leftrightarrow CH_3OH(g) + *$	0.53	0.40	3.6×10^{15}	2.1×10^3

[a]Pre-exponential factors are given for 500 K and are denoted A_f and A_b for forward and backward reactions, respectively. The pre-exponential factors are reported in s^{-1} for surface reactions and $Pa^{-1}\ s^{-1}$ for adsorption steps.

The barrier is low because of the surface electronic unfavorable situation with two OH groups upon H_2 adsorption. A Bader analysis upon CO_2 adsorption shows a charge transfer of 0.65 electron to the adsorbed molecule and a similar charge depletion on the In ion of adsorption. From this configuration, the formation of $COOH^-$ takes place by the transfer of one hydrogen atom from an OH group across the trench. The barrier for this step is 1.1 eV, this being the highest barrier in the catalytic cycle. The hydrogenation to $COOH^-$ is endothermic by 0.66 eV (Figure 3c). The reaction proceeds by rotation of $COOH^-$ changing the orientation of the OH group. The rotation is found to be slightly endothermic by 0.05 eV. The reaction proceeds by the scission of the CO−OH bond, yielding an adsorbed OH group at an In ion and a physisorbed CO molecule. The energy barrier of this process is 0.89 eV, and the reaction is exothermic by −0.36 eV. The desorption of the physisorbed CO is exothermic by −0.01 eV. The subsequent formation of water occurs by a proton transfer from a surface OH group to an In ion adsorbed OH group. The barrier for this step is 0.02 eV, and the process is exothermic by 0.03 eV. Finally, the desorption of water to the gas phase is endothermic by 0.54 eV. The water desorption includes the rearrangement of the surface to the initial configuration.

Kinetic Simulations. A mean-field microkinetic model was constructed from the DFT data to investigate the kinetic behavior of the investigated catalytic cycle. The considered elementary steps as well as the kinetic parameters (forward and backward activation energies and pre-exponential factors) are shown in Table 1.

The simulations were performed under typical methanol synthesis conditions: i.e., T = 423−673 K and p_x= 30:10:1:1:0 bar for $x = H_2{:}CO_2{:}H_2O{:}CH_3OH{:}CO$. In the model, hydrogen in the hydride (InH) and proton (OH) forms are lumped into one type of hydrogen. This should not be a severe approximation, given that the barrier between the states is small. The hydrogens in the OH groups within the initial 83% coverage were not included in the reported coverage. The surface coverages, turnover frequencies, and selectivities as a function of temperature are presented in Figure 4.

Coverage, Turnover Frequency, and Selectivity. At typical reaction temperatures the surface is predicted to be mainly covered by HCOO and OH groups and hydrogen (Figure 4a). On the basis of the thermodynamic analysis,[36,37] the surface was studied at a hydrogen coverage of 83% and the OH groups in the kinetic model and predicted coverage are OH groups originating from the catalytic cycles. The surface coverages indicate three temperature regimes. (i) The available surface sites are below 450 K mainly covered by OH groups. (ii) The surface is dominated by adsorbed HCOO in the temperature range 450−510 K. The coverage of HCOO peaks at 470 K, after which the number of free sites grows, signaling the takeoff of the methanol production. (iii) The surface above 510 K is dominated by free sites.

The turnover frequency as a function of temperature is presented in Figure 4b. The predicted methanol rate takes off at 470 K and reaches a maximum at 540 K, whereas the RWGS is the main reaction path above 580 K. This behavior is in qualitative agreement with experimental observations.[23−25] To our knowledge, this behavior has not been captured in previous microkinetic models for In_2O_3.[23,32,34]

The selectivity (Figure 4c) toward one of the reaction products is calculated as

$$S_x = \frac{r_x}{r_{CH_3OH} + r_{CO}} \tag{7}$$

The methanol selectivity is calculated to be high (0.68−0.94) in the temperature range from 420 to 500 K. The drop in methanol selectivity at the lowest temperatures is caused by the low rate of methanol formation coupled with the high coverage of OH groups on the surface, generated from H_2O splitting. The OH groups block adsorption sites for HCOO and hinder the conversion to methanol. The selectivity for methanol peaks at 480 K and decreases slowly to 0.75 at 540 K, which is the temperature where the methanol production has a maximum. At higher temperatures, the selectivity shifts toward the RWGS reaction, as expected from thermodynamics. In fact, in equilibrium, at 50 bar and a $H_2{:}CO_2$ ratio of 3:1, the selectivity for methanol is 90% at 510 K.[56] The predicted results for the selectivity are in agreement with experimental observations at low gas hourly space velocities.[12]

CO_2 Hydrogenation: Degree of Rate Control and Reaction Orders. The reaction orders and degree of rate control have been investigated to analyze the kinetic behavior and rate-limiting steps (Figure 5). The reaction orders are calculated under methanol synthesis conditions: T = 420−670 K and p_x = 30:10:1:1:0 bar for $x = H_2{:}CO_2{:}H_2O{:}CH_3OH{:}CO$. We

https://doi.org/10.1021/acscatal.1c01707
ACS Catal. 2021, 11, 9996−10006

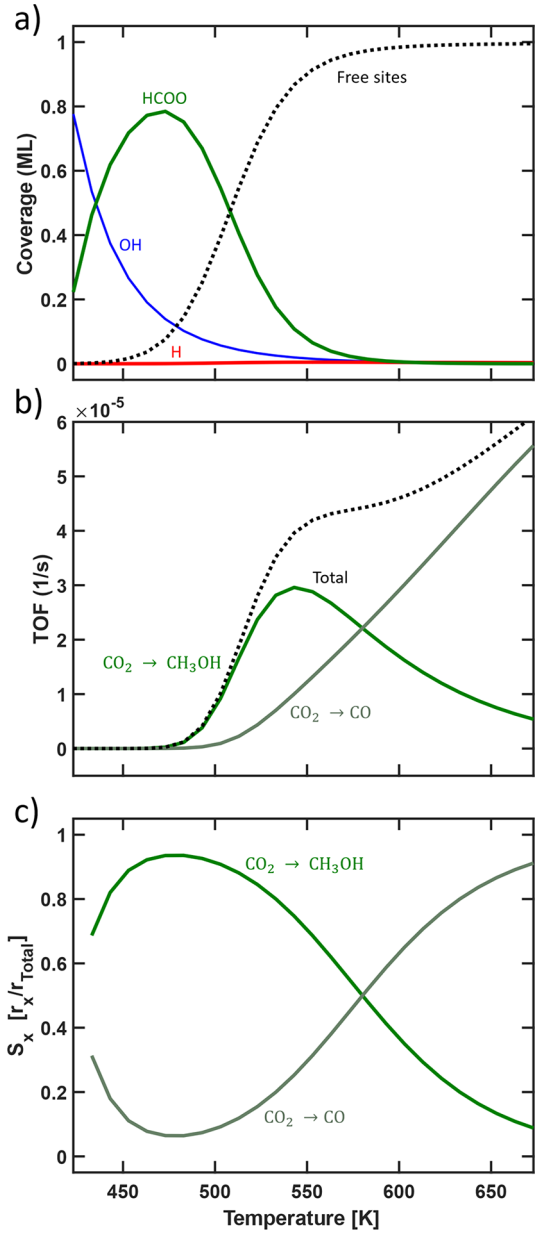

Figure 4. (a) Surface coverage, (b) Turnover frequency, and (c) Selectivity as a function of temperature. The simulations were performed at T = 423−673 K and p_x = 30:10:1:1:0 bar for x = H_2:CO_2:H_2O:CH_3OH:CO.

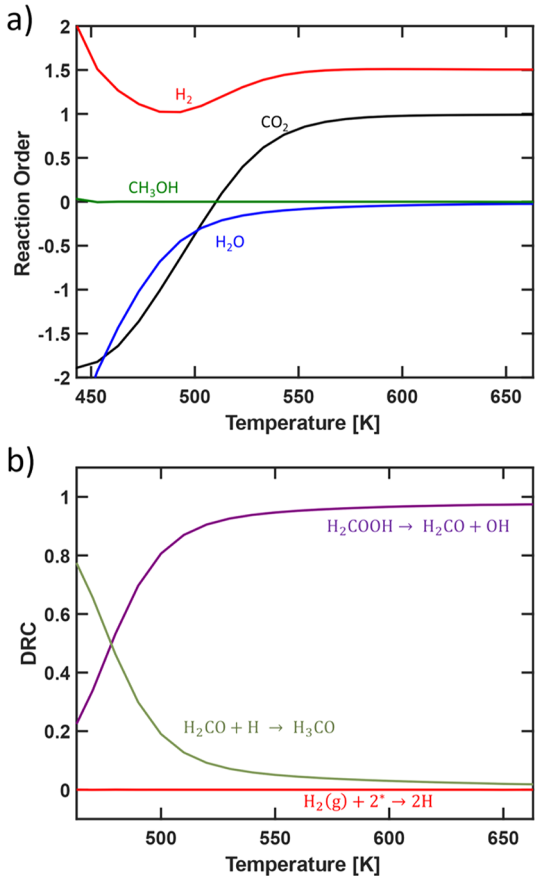

Figure 5. Temperature-dependent kinetic analysis of CO_2 hydrogenation to CH_3OH: (a) reaction orders of CO_2, H_2, H_2O, and CH_3OH; (b) degree of rate control. The simulations were performed under the same conditions as in Figure 4.

find that the reaction order of CO_2 varies from −1.9 to 1.0 in the investigated temperature range. The negative value at lower temperatures is a result of the high HCOO coverage. Thus, HCOO poisons the surface for the reaction to continue, as suggested from the surface coverages at the lower temperatures presented in Figure 3. At higher temperatures, the number of free sites increases, yielding a higher methanol production and a positive reaction order in CO_2 above 510 K. The reaction order in H_2 is more complex. It is ∼2 at low temperatures and decreases to ∼1 at $T \approx$ 470−500 K and thereafter increases to a value of 1.5 at high temperatures. The high value of n_{H_2} at low temperatures is caused by the adsorbed OH groups and the difficulty in reaching a sufficient hydrogen coverage. It should be noted that the reaction order in H_2 is always positive. Thus, an increased hydrogen coverage is always beneficial for methanol production. In contrast, the reaction order of H_2O is found to be negative, having a hindering effect on the methanol production because of site blocking at all temperatures. The H_2O reaction order spans from −2 to 0 in the probed temperature range. The reaction order of methanol is found to be 0 at all temperatures. Experimentally, the reaction orders have been measured to be n_{CO_2} = −0.1, n_{H_2} = 0.5−0.8, n_{H_2O} = −0.8, and n_{CH_3OH} = −0.2 at 573 K and P = 5 MPa.[24] The reaction orders in ref 24 were measured in the low-temperature regime, as the maximum rate of methanol production was measured to occur at 625 K. When a comparison is made with our results also ∼50 K below the methanol production maximum (500 K), the reaction orders are calculated to be n_{CO_2} = −0.26, n_{H_2} = 1.09, n_{H_2O} = −0.30, and n_{CH_3OH} = 0, thus in overall good agreement with the experiments.

To analyze the sensitivity of the calculated turnover frequency to each individual step in the reaction mechanism, the degree of rate control (χ_i) was calculated as a function of temperature. The results are presented in Figure 5b. The reaction is controlled by the dissociation of H_2COOH to H_2CO + OH and by the hydrogenation of H_2CO to H_3CO. At temperatures below 470 K, the rate is controlled mainly by the hydrogenation of H_2CO to H_3CO, whereas the rate is solely determined by the dissociation of H_2COOH to H_2CO at higher temperatures. This finding is consistent with the calculated energy barrier for both reaction steps (see Table 1). The activation energy for dissociative adsorption of H_2 does not have any significant rate

https://doi.org/10.1021/acscatal.1c01707
ACS Catal. 2021, 11, 9996−10006

control. Thus, a reduction in the energy barrier for hydrogen dissociation, without a change in the equilibrium constant, does not affect the activity, which is in contrast to interpretations of recent experiments.[24] The rate-controlling steps are found to be different from the case with Cu-based catalysts following the same mechanism.[57,58] The rate-controlling steps for Cu-based catalysts have been related to the hydrogenation of HCOO to HCOOH and to the hydrogenation of HCOOH to H_2COOH.

Reverse Water-Gas Shift Reaction: Degree of Rate Control and Reaction Orders. A kinetic analysis of the reaction orders and degree of rate control for the RWGS reaction is presented in Figure 6. The reaction orders were

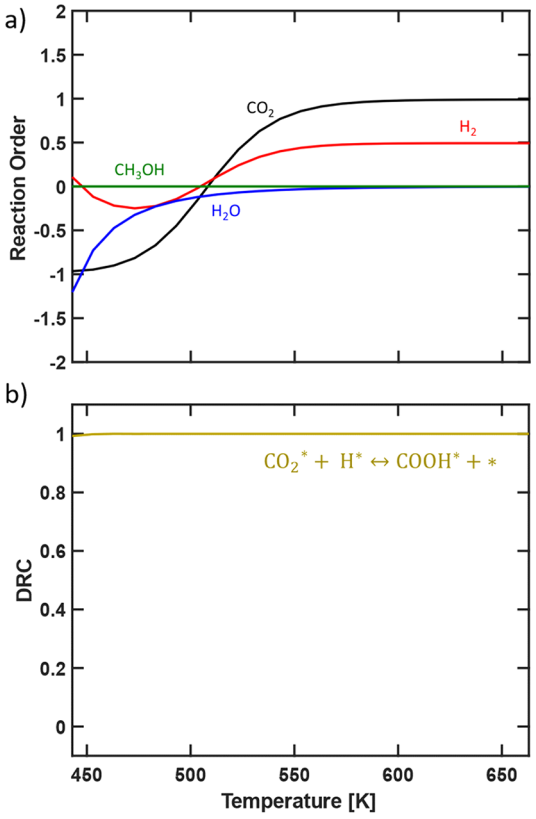

Figure 6. Temperature-dependent kinetic analysis of the RWGS reaction: (a) reaction orders of CO_2, H_2, H_2O, and CH_3OH; (b) degree of rate control. The simulations were performed under the same conditions as in Figure 4.

calculated under the same conditions as in the analysis of methanol formation. We find the reaction order of CO_2 to vary from −1.0 to 1.0 in the investigated temperature range. For methanol synthesis, the reaction order is negative at low temperatures as a result of HCOO surface poisoning. At higher temperatures, we notice that the reaction order reaches 1.0. The reaction order of hydrogen is significantly different from that of methanol synthesis, being negative at low temperatures with a minimum value of −0.25 at 470 K and reaching a limiting value of 0.5 at high temperatures. The negative value of the H_2 reaction order at low temperatures is a consequence of hydrogen consumption in the methanol synthesis reaction. The H_2 reaction order becomes positive at high temperatures as the reaction becomes thermodynamically favored. Similarly to methanol synthesis, the reaction order for water is negative, suggesting that water poisoning is detrimental for the catalytic activity of In_2O_3. The calculated reaction orders at 500 K are, −0.16, −0.02, −0.12, and 0 for CO_2, H_2, H_2O, and CH_3OH, respectively.

From an analysis of the degree of rate control (χ_i), we find that the RWGS rate is determined by CO_2 hydrogenation to COOH, which is consistent with the calculated energy barriers for the mechanism. This is in accord with the notion that the RWGS reaction is suppressed on In_2O_3.

DISCUSSION

The presented reaction network matches qualitatively the experimentally observed kinetic behavior of methanol synthesis over In_2O_3.[12,24] The simulated kinetic behavior for $In_2O_3(110)$ appears to be related to the stability and activation energy of HCOO and HCOOH. This is different from rate-controlling steps for methanol synthesis over Cu-based catalysts.[57,58] The difference in kinetic properties is probably a consequence of the lower activation energy for the HCOO → HCOOH hydrogenation (E_a = 0.72 eV), in comparison to that reported on pristine Cu(211) (E_a = 1.27 eV).[57] The barrier can also be compared with $In_2O_3(111)$, where the reported activation energy for HCOO → HCOOH is E_a = 1.32 eV.[23] The high activation energy for hydrogenation of HCOO is presumably related to the high stability of HCOO, as suggested in ref 57. The lower stability of HCOO in the present work in comparison to that in ref 23 is likely a consequence of the considered surface hydroxylation (in accord with the thermodynamic analysis).

O_v has not been considered in the present model. Given the agreement between our simulations and the experimental observations, the role of O_v is not evident. Moreover, the experimental abundance of oxygen vacancies is not completely clear. The concentration of vacancies has been assigned on the basis of XPS intensities, where a peak shifted ∼1.2 eV to higher energies with respect to the bulk peak has been attributed to oxygen ions close to oxygen vacancies.[12,25] However, our recent calculations indicate that oxygen vacancies do not result in significant shifts in O 1s binding energies.[30,37] Instead, we suggest that the signature shifting to higher binding energies could be attributed to different types of OH groups or, alternatively, different atomic structures. Our results suggest that oxygen vacancies, although thermodynamically stable at high operating temperatures,[36] are not required as active site enablers on $In_2O_3(110)$. It is possible that vacancies are needed on $In_2O_3(111)$ to activate the surface and facilitate changes in the oxidation state of the In ions. We note that it is undercoordinated In ions that have the ability to change oxidation state.[36]

From our analysis of the reaction orders and degree of rate control for hydrogen adsorption, it appears that the stabilization of hydrogen upon adsorption plays a significant role in methanol synthesis. To further interrogate the effect of the adsorbate stability on the turnover frequency for methanol, we investigated the sensitivity of the rate to the stability of the different adsorbates. This is done by stabilizing the adsorption energy of the reaction products for some reactions by 0.1 eV: i.e., changing the equilibrium constants. The results are presented in Figure 7.

We find that the most significant increase in methanol production rate is achieved by stabilizing the adsorption of hydrogen, where a 20-fold increase in the methanol rate is observed upon a 0.1 eV stabilization. This finding may elucidate the experimental observation of improved catalytic activity of ZrO_2-supported In_2O_3,[12] as In_2O_3 in this case is strained, and the observation that addition of Pd to In_2O_3 facilitates the reaction.[24,31] Although we find that the stabilization of surface

https://doi.org/10.1021/acscatal.1c01707
ACS Catal. 2021, 11, 9996−10006

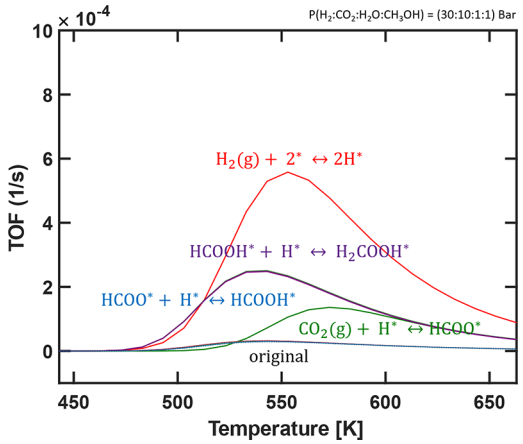

Figure 7. Change in the turnover frequency upon the stabilization of selected intermediates. The simulations were performed under the same conditions as in Figure 4.

hydrogen increases the rate, we do not find that the rate has a high sensitivity to the H_2 dissociation barrier.

CONCLUSIONS

We have used density functional theory calculations and mean-field microkinetic modeling to investigate CO_2 hydrogenation to CH_3OH on In_2O_3(110). The reaction mechanism includes a direct route for CO_2 hydrogenation to methanol and the competing reverse water-gas shift (RWGS) reaction. The hydrogenation path has been investigated along the route CO_2 → HCOO* → HCOOH* → H_2COOH* → H_2CO* → H_3CO* → CH_3OH* → CH_3OH. We find that the surface is covered mainly by HCOO, OH, and H at all temperatures. The turnover frequency for methanol production is found to take off at 470 K and reach a maximum at 540 K. The rate for methanol decreases at higher temperatures and is surpassed by the RWGS reaction at 580 K. The temperature dependence of the turnover frequencies is in qualitative agreement with experimental observations.[12] The reaction orders for the methanol synthesis (RWGS) reaction at 503 K are calculated to be −0.26 (−0.16), 1.09 (−0.02), and −0.30 (−0.12) for CO_2, H_2, and H_2O, respectively. The results for the reaction orders are in good agreement with experimental observations.[12]

CO_2 hydrogenation is found to be kinetically controlled by the H_2COOH dissociation to H_2CO + OH at all relevant reaction temperatures (470−670 K), whereas the RWGS is found to be solely determined by the hydrogenation of CO_2 to COOH. Shifting of the chemical equilibrium of the individual reaction steps reveals that the stabilization of hydrogen adsorption results in a significant increase in the methanol production.

The present work provides a fundamental understanding of the mechanistic aspects of CO_2 reduction to methanol on In_2O_3 surfaces and gives handles for the rational design of improved In_2O_3-based catalysts.

ASSOCIATED CONTENT

Supporting Information

The Supporting Information is available free of charge at https://pubs.acs.org/doi/10.1021/acscatal.1c01707.

Atomic structures, structural coordinates, procedure to correct energies of gas-phase species, and kinetic simulations without gas-phase corrections (PDF)

CIF files for the structures discussed in this paper (ZIP)

AUTHOR INFORMATION

Corresponding Authors

Alvaro Posada-Borbón − *Department of Physics and Competence Centre for Catalysis, Chalmers University of Technology, SE-412 96 Göteborg, Sweden*; Email: palvaro@chalmers.se

Henrik Grönbeck − *Department of Physics and Competence Centre for Catalysis, Chalmers University of Technology, SE-412 96 Göteborg, Sweden*; orcid.org/0000-0002-8709-2889; Email: ghj@chalmers.se

Complete contact information is available at: https://pubs.acs.org/10.1021/acscatal.1c01707

Notes

The authors declare no competing financial interest.

ACKNOWLEDGMENTS

A.P.-B. is grateful to Felix Hemmingsson for assistance with the Python implementation of the microkinetic model. Financial support from the Knut and Alice Wallenberg Foundation through the project "Atomistic design of catalysts" (No. KAW 2015.0058) is gratefully acknowledged. Additional support has been obtained from the Swedish Research Council (2020-05191) and the Swedish Energy Agency. The calculations have been performed at C3SE (Göteborg), Uppmax (Uppsala), and PDC (Stockholm) through a SNIC grant.

REFERENCES

(1) Olah, G. A. Beyond oil and gas: the methanol economy. *Angew. Chem., Int. Ed.* **2005**, *44*, 2636−2639.

(2) Olah, G. A.; Goeppert, A.; Prakash, G. K. S. Chemical recycling off carbon dioxide to methanol and dimethyl ether: from greenhouse gas to renewable, environmentally carbon neutral fuels and synthetic hydrocarbons. *J. Org. Chem.* **2009**, *74*, 487−498.

(3) Olah, G. A.; Prakash, G. K. S.; Goeppert, A. Anthropogenic chemical carbon cycle for a sustainable future. *J. Am. Chem. Soc.* **2011**, *133*, 12881−12898.

(4) Goeppert, A.; Czaun, M.; Jones, J.-P.; Prakash, G. K. S.; Olah, G. A. Recycling of carbon dioxide to methanol and derived products - closing the loop. *Chem. Soc. Rev.* **2014**, *43*, 7995−8048.

(5) Artz, J.; Mueller, T. E.; Thenert, K.; Kleinekorte, J.; Meys, R.; Sternberg, A.; Bardow, A.; Leitner, W. Sustainable Conversion of Carbon Dioxide: An Integrated Review of Catalysis and Life Cycle Assessment. *Chem. Rev.* **2018**, *118*, 434−504.

(6) Dresselhaus, M.; Thomas, I. Alternative energy technologies. *Nature* **2001**, *414*, 332−337.

(7) Grabow, L. C.; Mavrikakis, M. Mechanism of methanol synthesis on Cu through CO_2 and CO hydrogenation. *ACS Catal.* **2011**, *1*, 365−384.

(8) Behrens, M.; Studt, F.; Kasatkin, I.; Kuehl, S.; Haevecker, M.; Abild-Pedersen, F.; Zander, S.; Girgsdies, F.; Kurr, P.; Kniep, B.-L.; Tovar, M.; Fischer, R. W.; Nørskov, J. K.; Schlögl, R. The active site of methanol synthesis over $Cu/ZnO/Al_2O_3$ industrial catalysts. *Science* **2012**, *336*, 893−897.

(9) Graciani, J.; Mudiyanselage, K.; Xu, F.; Baber, A. E.; Evans, J.; Senanayake, S. D.; Stacchiola, D. J.; Liu, P.; Hrbek, J.; Fernandez Sanz, J.; Rodriguez, J. A. Highly active copper-ceria and copper-ceria-titania catalysts for methanol synthesis from CO_2. *Science* **2014**, *345*, 546−550.

(10) Studt, F.; Sharafutdinov, I.; Abild-Pedersen, F.; Elkjaer, C. F.; Hummelshøj, J. S.; Dahl, S.; Chorkendorff, I.; Nørskov, J. K. Discovery of a Ni-Ga catalyst for carbon dioxide reduction to methanol. *Nat. Chem.* **2014**, *6*, 320−324.

(11) Studt, F.; Behrens, M.; Kunkes, E. L.; Thomas, N.; Zander, S.; Tarasov, A.; Schumann, J.; Frei, E.; Varley, J. B.; Abild-Pedersen, F.; Nørskov, J. K.; Schlögl, R. The mechanism of CO and CO_2 hydrogenation to methanol over Cu-based catalysts. *ChemCatChem* **2015**, *7*, 1105−1111.
(12) Martin, O.; Martin, A. J.; Mondelli, C.; Mitchell, S.; Segawa, T. F.; Hauert, R.; Drouilly, C.; Curulla-Ferre, D.; Perez-Ramirez, J. Indium oxide as a superior catalyst for methanol synthesis by CO_2 hydrogenation. *Angew. Chem., Int. Ed.* **2016**, *55*, 6261−6265.
(13) Porosoff, M. D.; Yan, B.; Chen, J. G. Catalytic reduction of CO_2 by H_2 for synthesis of CO, methanol and hydrocarbons: challenges and opportunities. *Energy Environ. Sci.* **2016**, *9*, 62−73.
(14) Kattel, S.; Liu, P.; Chen, J. G. Tuning selectivity of CO_2 hydrogenation reactions at the metal/oxide interface. *J. Am. Chem. Soc.* **2017**, *139*, 9739−9754.
(15) Li, W.; Wang, H.; Jiang, X.; Zhu, J.; Liu, Z.; Guo, X.; Song, C. A short review of recent advances in CO_2 hydrogenation to hydrocarbons over heterogeneous catalysts. *RSC Adv.* **2018**, *8*, 7651−7669.
(16) Reichenbach, T.; Mondal, K.; Jaeger, M.; Vent-Schmidt, T.; Himmel, D.; Dybbert, V.; Bruix, A.; Krossing, I.; Walter, M.; Moseler, M. Ab initio study of CO_2 hydrogenation mechanisms on inverse ZnO/Cu catalysts. *J. Catal.* **2018**, *360*, 168−174.
(17) Hus, M.; Kopac, D.; Likozar, B. Catalytic hydrogenation of carbon dioxide to methanol: synergistic effect of bifunctional Cu/perovskite catalysts. *ACS Catal.* **2019**, *9*, 105−116.
(18) Pavlišič, A.; Huš, M.; Prašnikar, A.; Likozar, B. Multiscale modelling of CO_2 reduction to methanol over industrial Cu/ZnO/Al_2O_3 heterogeneous catalyst: Linking ab initio surface reaction kinetics with reactor fluid dynamics. *J. Cleaner Prod.* **2020**, *275*, 122958.
(19) Frei, M. S.; Mondelli, C.; García-Muelas, R.; Morales-Vidal, J.; Philipp, M.; Safonova, O. V.; López, N.; Stewart, J. A.; Ferré, D. C.; Pérez-Ramírez, J. Nanostructure of nickel-promoted indium oxide catalysts drives selectivity in CO_2 hydrogenation. *Nat. Commun.* **2021**, *12*, 1960.
(20) Kuld, S.; Conradsen, C.; Moses, P. G.; Chorkendorff, I.; Sehested, J. Quantification of Zinc Atoms in a Surface Alloy on Copper in an Industrial-Type Methanol Synthesis Catalyst. *Angew. Chem., Int. Ed.* **2014**, *53*, 5941−5945.
(21) Sun, J.; Metcalfe, I.; Sahibzada, M. Deactivation of Cu/ZnO/Al_2O_3 methanol synthesis catalyst by sintering. *Ind. Eng. Chem. Res.* **1999**, *38*, 3868−3872.
(22) Twigg, M.; Spencer, M. Deactivation of copper metal catalysts for methanol decomposition, methanol steam reforming and methanol synthesis. *Top. Catal.* **2003**, *22*, 191−203.
(23) Frei, M. S.; Capdevila-Cortada, M.; Garcia-Muelas, R.; Mondelli, C.; Lopez, N.; Stewart, J. A.; Ferre, D. C.; Perez-Ramirez, J. Mechanism and microkinetics of methanol synthesis via CO_2 hydrogenation on indium oxide. *J. Catal.* **2018**, *361*, 313−321.
(24) Frei, M. S.; Mondelli, C.; Garcia-Muelas, R.; Kley, K. S.; Puertolas, B.; Lopez, N.; Safonova, O. V.; Stewart, J. A.; Ferre, D. C.; Perez-Ramirez, J. Atomic-scale engineering of indium oxide promotion by palladium for methanol production via CO_2 hydrogenation. *Nat. Commun.* **2019**, *10*, 3377.
(25) Frei, M. S.; Mondelli, C.; Cesarini, A.; Krumeich, F.; Hauert, R.; Stewart, J. A.; Curulla Ferré, D.; Pérez-Ramírez, J. Role of Zirconia in Indium Oxide-Catalyzed CO_2 Hydrogenation to Methanol. *ACS Catal.* **2020**, *10*, 1133−1145.
(26) Tsoukalou, A.; Abdala, P. M.; Stoian, D.; Huang, X.; Willinger, M.-G.; Fedorov, A.; Mueller, C. R. Structural evolution and dynamics of an In_2O_3 catalyst for CO_2 hydrogenation to methanol: An operando XAS-XRD and In situ TEM study. *J. Am. Chem. Soc.* **2019**, *141*, 13497−13505.
(27) Tsoukalou, A.; Abdala, P. M.; Armutlulu, A.; Willinger, E.; Fedorov, A.; Müller, C. R. Operando X-ray Absorption Spectroscopy Identifies a Monoclinic ZrO_2:In Solid Solution as the Active Phase for the Hydrogenation of CO_2 to Methanol. *ACS Catal.* **2020**, *10*, 10060−10067.
(28) Chou, C.-Y.; Lobo, R. F. Direct conversion of CO_2 into methanol over promoted indium oxide-based catalysts. *Appl. Catal., A* **2019**, *583*, 117144.
(29) Ye, J.; Liu, C.; Mei, D.; Ge, Q. Active oxygen vacancy site for methanol synthesis from CO_2 hydrogenation on In_2O_3(110): a DFT study. *ACS Catal.* **2013**, *3*, 1296−1306.
(30) Posada-Borbón, A.; Bosio, N.; Grönbeck, H. On the signatures of oxygen vacancies in O1s core level shifts. *Surf. Sci.* **2021**, *705*, 121761.
(31) Yang, C.; Pei, C.; Luo, R.; Liu, S.; Wang, Y.; Wang, Z.; Zhao, Z.-J.; Gong, J. Strong Electronic Oxide−Support Interaction over In_2O_3/ZrO_2 for Highly Selective CO_2 Hydrogenation to Methanol. *J. Am. Chem. Soc.* **2020**, *142*, 19523−19531.
(32) Zhou, Z.; Qin, B.; Li, S.; Sun, Y. A DFT-based microkinetic study on methanol synthesis from CO_2 hydrogenation over the In_2O_3 catalyst. *Phys. Chem. Chem. Phys.* **2021**, *23*, 1888−1895.
(33) Dang, S.; Qin, B.; Yang, Y.; Wang, H.; Cai, J.; Han, Y.; Li, S.; Gao, P.; Sun, Y. Rationally designed indium oxide catalysts for CO_2 hydrogenation to methanol with high activity and selectivity. *Sci. Adv.* **2020**, *6*, No. eaaz2060.
(34) Qin, B.; Zhou, Z.; Li, S. Reaction pathways and the role of the carbonates during CO_2 hydrogenation over hexagonal In_2O_2 catalysts. *Appl. Surf. Sci.* **2021**, *542*, 148591.
(35) Wagner, M.; Seiler, S.; Meyer, B.; Boatner, L. A.; Schmid, M.; Diebold, U. Reducing the In_2O_3 (111) surface results in ordered indium adatoms. *Adv. Mater. Interfaces* **2014**, *1* (8), 1400289.
(36) Posada-Borbón, A.; Grönbeck, H. CO_2 adsorption on hydroxylated In_2O_3(110). *Phys. Chem. Chem. Phys.* **2019**, *21*, 21698−21708.
(37) Posada-Borbón, A.; Grönbeck, H. Hydrogen adsorption on In_2O_3(111) and In_2O_3(110). *Phys. Chem. Chem. Phys.* **2020**, *22*, 16193−16202.
(38) Kresse, G.; Hafner, J. Ab initio molecular dynamics for liquid metals. *Phys. Rev. B: Condens. Matter Mater. Phys.* **1993**, *47*, 558−561.
(39) Kresse, G.; Hafner, J. Ab initio molecular-dynamics simulation of the liquid-metal-amorphous-semiconductor transition in Germanium. *Phys. Rev. B: Condens. Matter Mater. Phys.* **1994**, *49*, 14251−14269.
(40) Kresse, G.; Furthmüller, J. Efficiency of ab-initio total energy calculations for metals and semiconductors using a plane-wave basis set. *Comput. Mater. Sci.* **1996**, *6*, 15−50.
(41) Kresse, G.; Furthmüller, J. Efficient iterative schemes for ab initio total-energy calculations using a plane-wave basis set. *Phys. Rev. B: Condens. Matter Mater. Phys.* **1996**, *54*, 11169−11186.
(42) Perdew, J. P.; Burke, K.; Ernzerhof, M. Generalized gradient approximation made simple. *Phys. Rev. Lett.* **1996**, *77*, 3865−3868.
(43) Blochl, P. E. Projector augmented-wave method. *Phys. Rev. B: Condens. Matter Mater. Phys.* **1994**, *50*, 17953−17979.
(44) Kresse, G.; Joubert, D. From ultrasoft pseudopotentials to the projector augmented-wave method. *Phys. Rev. B: Condens. Matter Mater. Phys.* **1999**, *59*, 1758−1775.
(45) Monkhorst, H. J.; Pack, J. D. Special points for Brillouin-zone integrations. *Phys. Rev. B* **1976**, *13*, 5188−5192.
(46) Henkelman, G.; Uberuaga, B.; Jonsson, H. A climbing image nudged elastic band method for finding saddle points and minimum energy paths. *J. Chem. Phys.* **2000**, *113*, 9901−9904.
(47) Peterson, A. A.; Abild-Pedersen, F.; Studt, F.; Rossmeisl, J.; Nørskov, J. K. How copper catalyzes the electroreduction of carbon dioxide into hydrocarbon fuels. *Energy Environ. Sci.* **2010**, *3*, 1311−1315.
(48) Granda-Marulanda, L. P.; Rendón-Calle, A.; Builes, S.; Illas, F.; Koper, M. T. M.; Calle-Vallejo, F. A Semiempirical Method to Detect and Correct DFT-Based Gas-Phase Errors and Its Application in Electrocatalysis. *ACS Catal.* **2020**, *10*, 6900−6907.
(49) Virtanen, P.; Gommers, R.; Oliphant, T. E.; Haberland, M.; Reddy, T.; Cournapeau, D.; Burovski, E.; Peterson, P.; Weckesser, W.; Bright, J.; van der Walt, S. J.; Brett, M.; Wilson, J.; Millman, K. J.; Mayorov, N.; Nelson, A. R. J.; Jones, E.; Kern, R.; Larson, E.; Carey, C. J.; Polat, İ.; Feng, Y.; Moore, E. W.; VanderPlas, J.; Laxalde, D.; Perktold, J.; Cimrman, R.; Henriksen, I.; Quintero, E. A.; Harris, C. R.; Archibald, A. M.; Ribeiro, A. H.; Pedregosa, F.; van Mulbregt, P. SciPy

https://doi.org/10.1021/acscatal.1c01707
ACS Catal. 2021, 11, 9996−10006

1.0 Contributors, SciPy 1.0: Fundamental Algorithms for Scientific Computing in Python. *Nat. Methods* **2020**, *17*, 261−272.
(50) Chorkendorff, I.; Niemantsverdriet, J. W. *Concepts of Modern Catalysis and Kinetics*, 3rd ed.; Wiley-VCH: 2017.
(51) Linstrom, P. J.; Mallard, W. G. *NIST Chemistry WebBook; NIST Standard Reference Database Number 69*; National Institute of Standards and Technology; http://webbook.nist.gov, 2005 (Online; accessed December 11, 2020).
(52) Eyring, H. The Activated Complex in Chemical Reactions. *J. Chem. Phys.* **1935**, *3*, 107−115.
(53) Campbell, C. T. The Degree of Rate Control: A Powerful Tool for Catalysis Research. *ACS Catal.* **2017**, *7*, 2770−2779.
(54) Bielz, T.; Lorenz, H.; Jochum, W.; Kaindl, R.; Klauser, F.; Kloetzer, B.; Penner, S. Hydrogen on In_2O_3: reducibility, bonding, defect formation, and reactivity. *J. Phys. Chem. C* **2010**, *114*, 9022−9029.
(55) Van den Bossche, M.; Grönbeck, H. Adsorbate Pairing on Oxide Surfaces: Influence on Reactivity and Dependence on Oxide, Adsorbate Pair and Density Functional. *J. Phys. Chem. C* **2017**, *121*, 8390.
(56) Stangeland, K.; Li, H.; Yu, Z. Thermodynamic analysis of chemical and phase equilibria in CO_2 hydrogenation to methanol, dimethyl ether, and higher alcohols. *Ind. Eng. Chem. Res.* **2018**, *57*, 4081−4094.
(57) Wu, P.; Yang, B. Significance of Surface Formate Coverage on the Reaction Kinetics of Methanol Synthesis from CO_2 Hydrogenation over Cu. *ACS Catal.* **2017**, *7*, 7187−7195.
(58) Mao, Z.; Campbell, C. T. Apparent Activation Energies in Complex Reaction Mechanisms: A Simple Relationship via Degrees of Rate Control. *ACS Catal.* **2019**, *9*, 9465−9473.

https://doi.org/10.1021/acscatal.1c01707
ACS Catal. 2021, 11, 9996−10006